

Short-Time Infrequent Metadynamics for Improved Kinetics Inference

Ofir Blumer,[†] Shlomi Reuveni,^{†,‡,¶} and Barak Hirshberg^{*,†,‡,¶}

[†]*School of Chemistry, Tel Aviv University, Tel Aviv 6997801, Israel.*

[‡]*The Center for Computational Molecular and Materials Science, Tel Aviv University, Tel Aviv 6997801, Israel.*

[¶]*The Center for Physics and Chemistry of Living Systems, Tel Aviv University, Tel Aviv 6997801, Israel.*

E-mail: hirshb@tauex.tau.ac.il

Abstract

Infrequent Metadynamics is a popular method to obtain the rate of long timescale processes from accelerated simulations. The inference procedure is based on rescaling the first-passage times of Metadynamics trajectories using a bias-dependent acceleration factor. While useful in many cases, it is limited to Poisson kinetics, and a reliable estimation of the unbiased rate requires slow bias deposition and prior knowledge of efficient collective variables. Here, we propose an improved inference scheme, which is based on two key observations: 1) The time-independent rate of Poisson processes can be estimated using short trajectories only. 2) Short trajectories experience minimal bias, and their rescaled first-passage times follow the unbiased distribution even for relatively high deposition rates and suboptimal collective variables. Therefore, by limiting the inference procedure to short timescales, we obtain an improved tradeoff between speedup and accuracy at no additional computational cost, especially when employing suboptimal collective variables. We demonstrate the improved inference scheme for a model system and two molecular systems.

Molecular dynamics (MD) simulations are widely used to study complex systems at the microscopic level. Their atomic resolution allows evaluating thermodynamic and kinetic properties, but also limits the accessible timescales.^{1–4} Therefore, long timescale processes, such as protein folding or crystal nucleation, are almost never studied using brute-force, long simulations.⁵ Instead, enhanced sampling methods are usually employed.

Various methods were developed to study long timescale processes through MD simulations. Some use a series of short simulations to sample the unbiased kinetics, such as milestoning,^{6,7} Markov state models,^{8,9} stochastic resetting^{10,11} and many others. Another approach is to introduce an external bias potential, enhancing the sampling along a low dimensional collective variables (CVs) space. The chosen CVs are usually slow modes that can distinguish between metastable states.^{1–5} Methods following this approach include umbrella sampling,^{12,13} conformational flooding,¹⁴ adiabatic free energy dynamics,^{15–17} On-the-fly Probability Enhanced Sampling (OPES),^{18,19} Metadynamics (MetaD)^{3,20,21} and more.

Here, we focus on infrequent MetaD (iMetaD), a method to extract the unbiased kinetics from accelerated MetaD simulations. In iMetaD, several biased trajectories are initiated and stopped after a first-passage criterion is fulfilled. The first-passage time (FPT) of each trajectory is then rescaled by an acceleration factor that depends on the external bias deposited along the trajectory.¹ The method assumes that the underlying process obeys Poisson kinetics, and the unbiased rate is estimated by fitting the rescaled FPTs to an exponential distribution.²

The key assumption of iMetaD is that no bias is deposited near the transition state.^{1,5} This assumption fails for high bias deposition rates or suboptimal CVs, that lead to hysteresis and bias over-deposition.^{2,5,22} Unfortunately, finding good CVs in complex systems remains a great challenge,^{23,24} despite recent developments.^{25–31} Thus, to improve the inference, one is usually forced to limit the bias deposition rate but this also reduces the acceleration, resulting in a tradeoff between speedup and accuracy.^{4,11,22}

The reliability of iMetaD is usually assessed through a procedure suggested by Salvalagio

et. al.^{2,5} A Kolmogorov–Smirnov (KS) test³² is performed to accept or reject the hypothesis that the rescaled FPTs are taken from an exponential distribution. The results are considered reliable for a p-value greater than 0.05, and the unbiased mean FPT (MFPT) is then estimated as the mean of the exponential fit to the rescaled FPT distribution. Trajectories with hysteresis or over-deposition contribute unrealistically long rescaled FPTs, leading to distributions that are broader than exponential and failure of the KS test. In this paper, we propose an improved inference scheme which deals with this prevalent problem, extending the range of applicability of iMetaD.

The scheme relies on two key observations: 1) Since exponential distributions are characterized by a single parameter – their time-independent kinetic rate – short simulations, showing a single transition each, are sufficient to estimate the full distribution reliably. 2) The rescaling procedure of iMetaD is more reliable for short trajectories, experiencing minimal bias. This can be seen from the rescaled FPT distribution, which often follows the unbiased distribution at short times even when using high bias deposition rates or suboptimal CVs. The improved scheme is inspired by our previous work, combining MetaD with stochastic resetting (SR).¹¹ Previously, we showed that SR provides enriched the sampling of short timescales, leading to an improved tradeoff between speedup and accuracy. Interestingly, these observations are not limited to simulations with SR.

We next show how to exploit our observations to build an improved kinetics inference scheme for iMetaD simulations. We refer to this scheme as Short Time iMetaD (ST-iMetaD). ST-iMetaD extends the applicability of iMetaD even to high bias deposition rates and suboptimal collective variables, reducing the prediction errors by orders of magnitude in comparison to the standard procedure. We demonstrate its advantages in three systems of increasing complexity: the two-dimensional Wolfe-Quapp potential, alanine dipeptide in vaccum, and the unfolding of the chignolin mini-protein in water.

We present ST-iMetaD through the example of the Wolfe-Quapp potential. It is a two states model, previously used to study the performance of suboptimal CVs.^{22,23} Its exact

form is given in the SI, as well as all simulations details. We first performed brute-force, standard MD simulations, to obtain the unbiased FPT distribution, and found the MFPT to be $\sim 110\text{ ns}$. A KS test confirmed that the unbiased distribution is exponential (a p-value of 0.81).

Next, we performed iMetaD simulations with a good CV and slow bias deposition rate of 10 ns^{-1} , updating the bias every 10^5 timesteps. The quality of the CV was proved using committor analysis^{33,34} (see SI for details). With this choice of parameters, we expect the underlying assumptions of iMetaD to be valid, and the original inference scheme to be accurate. Indeed, the MFPT estimated through the standard inference procedure is 121 ns , in good agreement with the true value. A p-value of 0.31 confirms the reliability of the results. The left panel of Figure 1(a) shows the cumulative distribution functions (CDF) $P(\tau \leq t)$ for both the unbiased FPTs (blue solid line) and the rescaled FPTs (green dashed line). An exponential fit to the CDF of the rescaled FPTs is given in an orange dash-dotted line. We find a good agreement between all three curves, showing that the standard inference procedure is adequate in this case.

We then performed iMetaD simulations using the same CV but with a higher bias deposition rate of 1000 ns^{-1} (every 1000 timesteps), which is expected to give poor inference due to hysteresis. The obtained MFPT, 1031 ns , overestimates the true value by an order of magnitude, and the p-value of the KS test drops to 5×10^{-7} , indicating that the results are unreliable. The middle panel of Figure 1(a) again shows the CDF for the unbiased and rescaled FPTs, as well as the exponential fit to the rescaled CDF. In this case, we find that the rescaled CDF is not exponential and clearly deviates from the unbiased CDF. As a result, the exponential fit results in a wrong estimate of the rate and MFPT. Nevertheless, we find that the unbiased and rescaled CDFs are in very close agreement at short times. This is the first key observation of this work: short trajectories experience minimal bias and thus their rescaled CDF reflects the correct statistics for small FPTs even at high bias deposition rates.

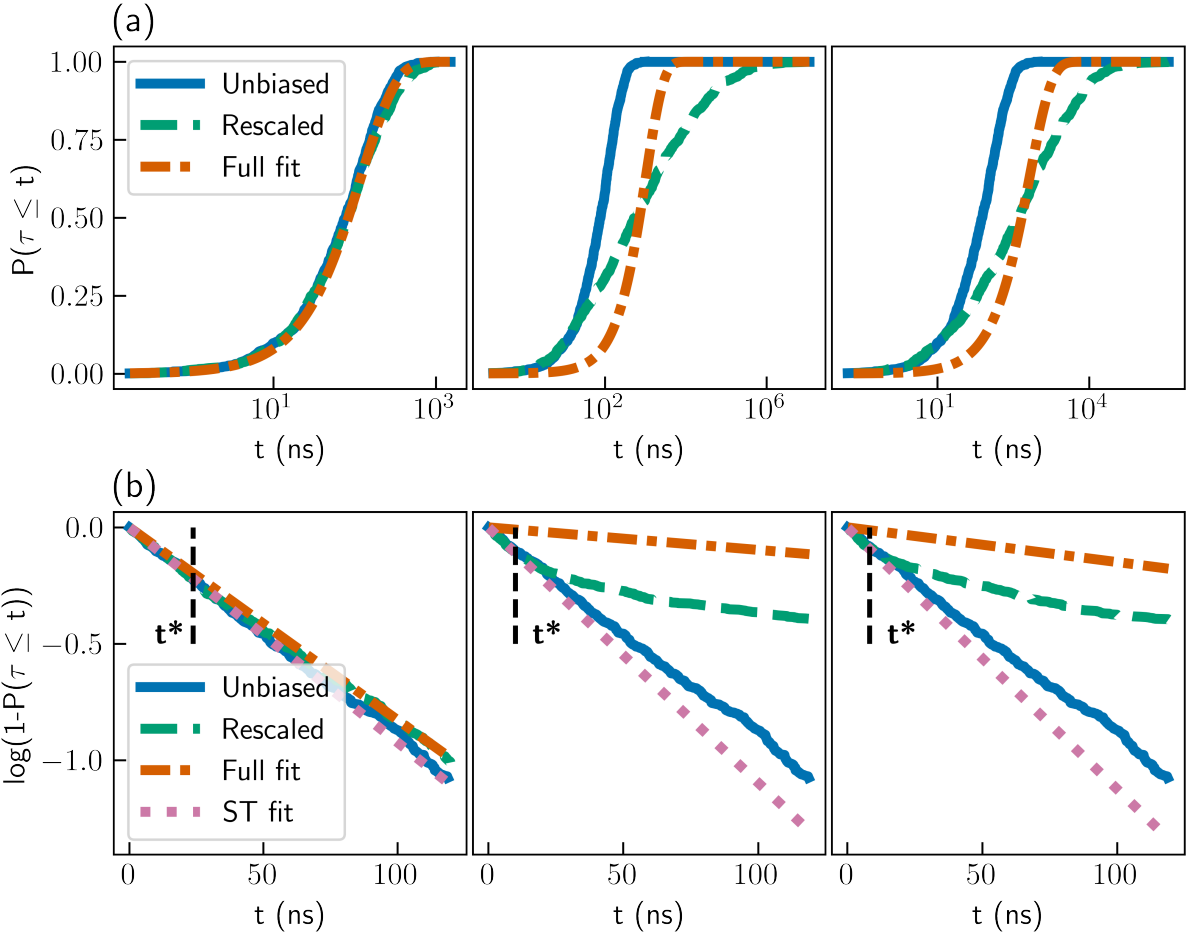


Figure 1: (a) CDF profiles and (b) survival functions for simulations of the Wolfe-Quapp potential. Results for unbiased FPTs (blue solid lines), rescaled FPTs (dashed green lines), exponential fits to the rescaled CDF in the entire range (orange dash-dotted lines), and linear fits to the survival functions at $t < t^*$ (pink dotted lines). Results are shown for iMetaD simulations using a good CV and bias deposition rate of 10 ns^{-1} (left), a good CV and bias deposition rate of 1000 ns^{-1} (middle) and a suboptimal CV and bias deposition rate of 200 ns^{-1} (right). The black dashed lines mark $t = t^*$.

A similar phenomenon is observed when employing suboptimal CVs. We select a moderate bias deposition rate of 200 ns^{-1} , and intentionally reduce the quality of the CV by rotating it at an angle $\theta = 56^\circ$ relative to the good CV. The right panel of Figure 1(a) presents the resulting CDF profiles. Once again, the rescaled CDF is far from exponential (p-value of 6×10^{-6}), and the MFPT is overestimated ($\sim 670\text{ ns}$). However, even though the rescaled CDF deviates from the unbiased CDF at long times, they match closely at short

times.

When employing iMetaD, it is common practice to present the rescaled CDF profile, which is used for the KS test.^{2,4,5} However, for the rest of this paper, it would be more convenient to examine the survival function, $1 - P(\tau \leq t)$, since its logarithm decays linearly for exponential distributions. Figure 1(b) gives $\log(1 - P(\tau \leq t))$ for the unbiased FPTs (blue solid lines) and for the rescaled FPTs (green dashed lines) of the simulations presented in Figure 1(a). The unbiased survival function decays linearly, as expected. When the assumptions of iMetaD hold (left panel), the rescaled survival function closely follows the unbiased one. When they break (middle and right panels), the rescaled survival function matches the unbiased one up to some finite time $t = t^*$, and decays slower at $t > t^*$. As a result, the exponential fits to the rescaled data (orange dash-dotted lines) decay much slower than the unbiased curves. This explains the overestimated MFPT values.

We improve the inference by fitting a linear function $S(t) = -kt$ to the rescaled survival function at $t \leq t^*$ only (dotted pink lines in Figure 1(b)). We then estimate the MFPT as k^{-1} . Notice that we only fit a single parameter k , as the survival function must fulfill $S(t = 0) = 0$ due to normalization. In all three cases, we find that these short-time fits are closer to the unbiased survival function, and therefore lead to an improved estimate of the MFPT, as we show below. First, we explain how to choose an adequate value of t^* .

We use the Pearson correlation coefficient R , which quantifies the quality of the linear fit to the survival function. Practically, we perform multiple fittings, with different choices of t^* , and select the fit resulting in the highest value of R^2 . Our results show that this approach correctly identifies reasonable values of t^* , such that the rescaled survival functions match the unbiased ones at $t \leq t^*$. Specifically, for a good CV and a low bias deposition rate, where the results are reliable, we find $t^* \sim 24\text{ ns}$. For the same CV and a high bias deposition rate, and for a poor CV and a moderate rate, we obtain lower values, $t^* \sim 10\text{ ns}$ and $t^* \sim 8\text{ ns}$, respectively (black dashed lines in Figure 1(b)).

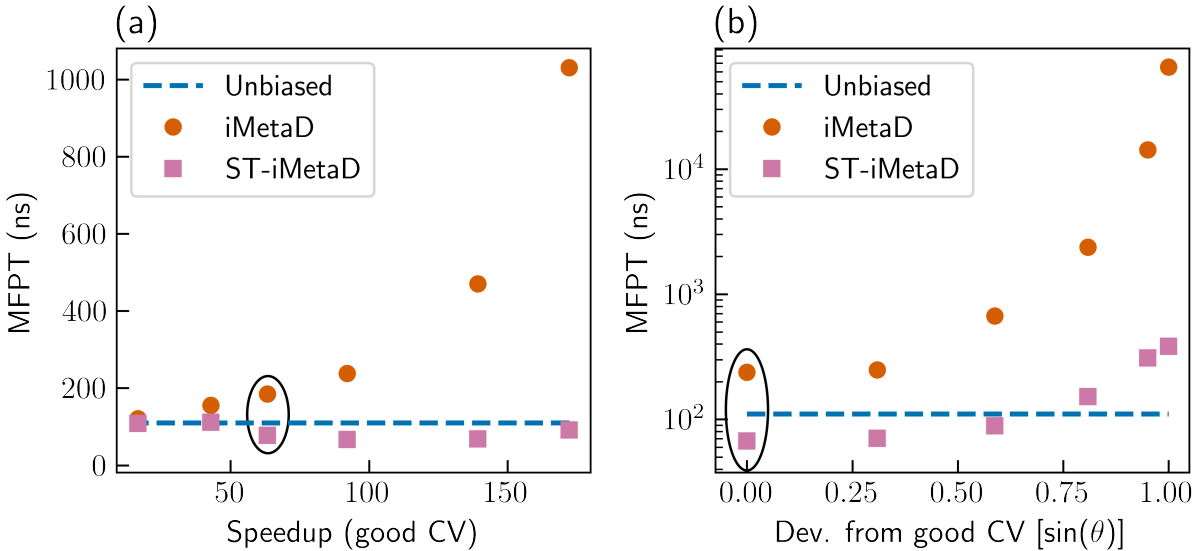


Figure 2: (a) Estimated MFPTs as a function of the speedup for the Wolfe-Quapp potential using a good CV and different bias deposition rates from 10 to 1000 ns^{-1} . (b) Estimated MFPTs for a bias deposition rate of 200 ns^{-1} , and different choices of CV. The blue lines mark the unbiased MFPT value. We employed either standard iMetaD (orange circles) or ST-iMetaD (pink squares). The black ellipses highlight overlapping points in the two panels.

To summarize our method, the main modification to the original inference scheme is that instead of fitting an exponential distribution to all of the data, as customary, we limit the analysis to short timescales. We perform a series of linear fits to the logarithm of the survival function at times $t \leq t^*$, with different choices of t^* . The parameter k of the best fit is taken as the kinetic rate, and the MFPT is estimated as k^{-1} . This enables accurate estimations of the MFPT, even with frequent bias deposition or a suboptimal CV.

We first demonstrate the advantages of ST-iMetaD using the Wolfe-Quapp potential, showing that we can use higher bias deposition rates, providing higher speedups, with minimal penalty in the inference accuracy. Figure 2(a) shows the estimated MFPT as a function of the speedup, using a good CV and different bias deposition rates in the range of 10 to 1000 ns^{-1} . When employing standard iMetaD (orange circles), the estimated MFPT increases with speedup, reaching a value that is an order of magnitude larger than the true one at high speedups. On the other hand, when employing ST-iMetaD (pink squares), we

obtain estimations within 40% of the true value, for all speedups.

Our scheme also improves the inference from simulations performed with suboptimal CVs. For a fixed bias deposition rate of 200 ns^{-1} , we gradually reduce the quality of the CV by rotating it with respect to the good CV. Figure 2(b) shows that the estimated MFPT increases as the quality of the CV decreases, for both inference schemes. However, the deviation from the true value is much smaller for ST-iMetaD. The errors remain within an order of magnitude of the true value, in comparison to more than two orders of magnitude for standard iMetaD, even for very poor CVs. We note that with ST-iMetaD, the predicted MFPT may also be slightly underestimated, but remains close to the true value.

We next apply ST-iMetaD in two molecular systems, starting with the well-studied example of alanine dipeptide in vacuum. Alanine dipeptide has two stable conformers, C_{7eq} and C_{7ax} , and is usually described by two dihedral angles, ϕ and ψ , with ϕ serving as a good CV and ψ as a suboptimal one^{1,2,18,22} (see Ref.¹ for definitions of conformers and angles). Transitions from the C_{7eq} conformer to the C_{7ax} conformer have an estimated MFPT of $\sim 3.5\text{ }\mu\text{s}$ (see SI for more details). We performed MetaD simulations with bias deposition rates in the range of 20 to 1000 ns^{-1} , and either the ϕ or ψ angle as CV. Full simulations details are given in the SI.

Figure 3(a) shows the estimated MFPT as a function of the speedup for simulations biasing the ϕ angle, through the original iMetaD scheme (orange circles) and ST-iMetaD (pink squares). The unbiased MFPT is given in a dashed blue line. The two schemes provide similar, very accurate estimations, even with frequent bias deposition. This confirms that ST-iMetaD is consistent with standard iMetaD, when the latter is reliable.

On the other hand, when ψ , a suboptimal CV, is employed we find a major difference between the schemes, as demonstrated in Figure 3(b). With standard iMetaD (orange circles), the estimated MFPT rapidly increases with speedup (notice the logarithmic scale). It varies from a value of $15.8\text{ }\mu\text{s}$ at a bias deposition rate of 20 ns^{-1} up to $9930\text{ }\mu\text{s}$ at a rate of 1000 ns^{-1} , an error of more than three orders of magnitude. However, with ST-iMetaD,

we obtain estimations that fall in a much smaller range, $2.0 - 13.6 \mu s$, within an order of magnitude from the true value.

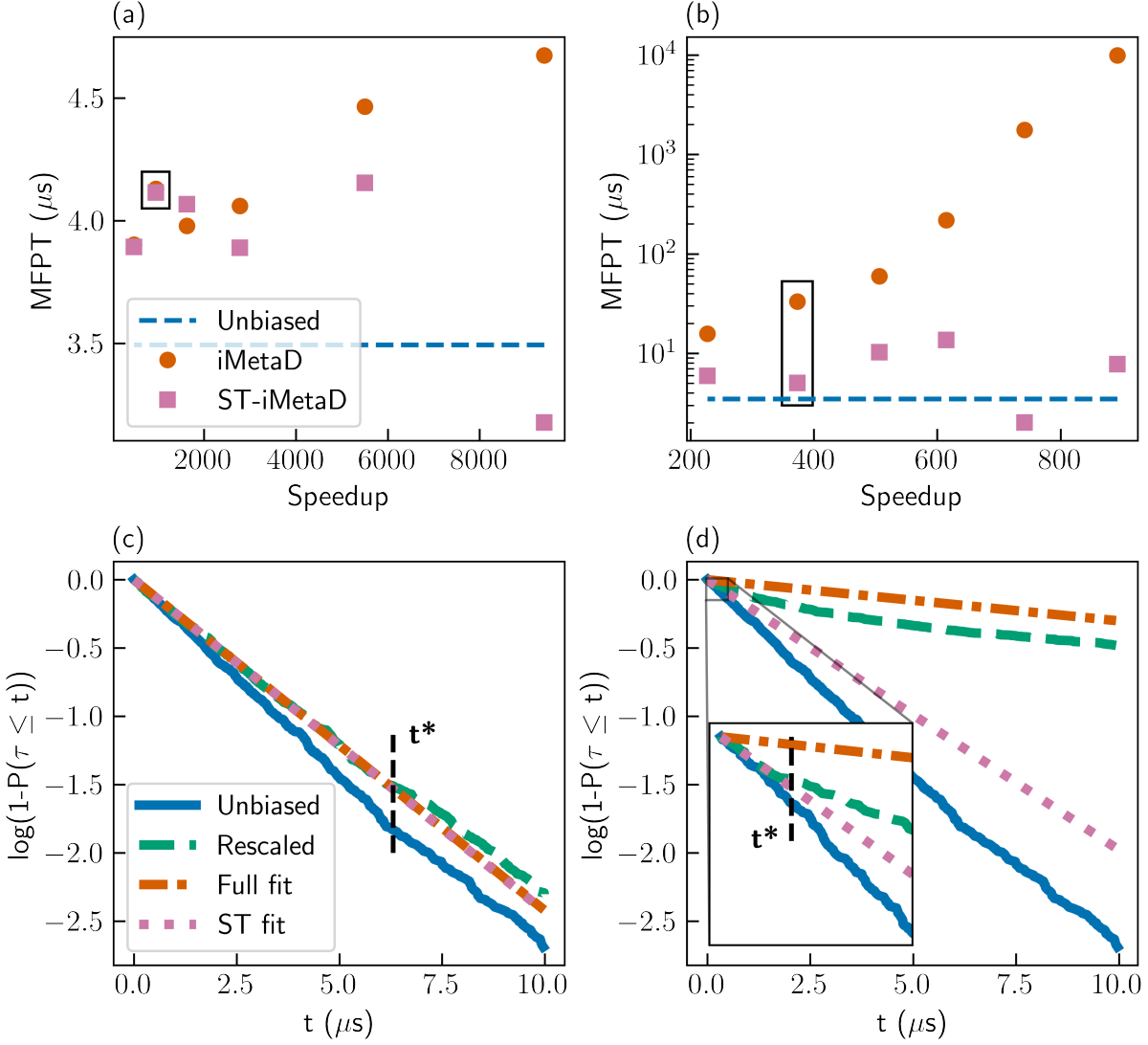


Figure 3: Upper row: Estimation of the MFPT as a function of speesup, for the $C_{7eq} - C_{7ax}$ conformer transition of alanine dipeptide in vacuum. Simulations using either (a) the ϕ angle or (b) the ψ angle as CV, with the originial inference scheme (orange circles) or the improved one (pink squares). The black rectangles highlight result obtained with bias deposition rate of 50 ns^{-1} . Lower row: Survival functions $\log(1 - P(\tau \leq t))$ for unbiased simulations (blue solid lines) and rescaled iMetaD simulations (green dashed lines), biasing either the (c) ϕ angle or (d) ψ angle, with bias deposition rate of 50 ns^{-1} . Additional lines show the fit obtained using the original scheme (orange, dash-dotted) and the improved scheme (pink, dotted). The black dashed lines mark $t = t^*$. The inset in panel (d) zooms-in on $t < 0.5 \mu s$.

We validate the underlying assumptions of ST-iMetaD by examining the survival functions. Panels (c) and (d) of Figure 3 show the survival functions for the unbiased FPT distribution (solid blue lines), the rescaled FPT distributions (dashed green lines), the fit of iMetaD (dash-dotted orange lines) and the fit of ST-iMetaD (pink dotted lines). Results are shown for simulations with a moderate bias deposition rate of 50 ns^{-1} , which is standard for iMetaD.^{1,2} The MFPT estimations using this rate are highlighted with black rectangles in panels (a) and (b). Using the ϕ angle as CV, the rescaled survival function decays at a similar rate as the unbiased one (panel (c)). We determine $t^* = 6.3\text{ }\mu\text{s}$ using the procedure described before, and the two fits coincide. Using the ψ angle as CV, the rescaled survival function quickly deviates from the unbiased one (panel (d)). Nevertheless, they match at short times, as visible in the inset, which zooms-in on $t \leq 0.5\text{ }\mu\text{s}$. We determine a value of $t^* = 184\text{ ns}$, and reduce the error in the predicted MFPT by a factor of ~ 6.5 .

We close this paper with a more complex example – the unfolding of chignolin in explicit water (simulations of 5889 atoms). Chignolin is a mini-protein composed of 10 amino acids,³⁵ previously used to benchmark enhanced sampling methods.^{11,22,36–38} A linear combination of six interatomic contacts, optimized via harmonic linear discriminant analysis (HLDA) by Mendels et. al.,²⁵ serves as a good CV. The radius of gyration (Rg) and the C-alpha root-mean-square deviation from a folded configuration (RMSD) serve as examples of suboptimal CVs. All simulation details are provided in the SI.

Figure 4(a) gives the free-energy surfaces (FES) along all CVs, obtained from umbrella sampling simulations (see SI for details) using the weighted histogram analysis method (WHAM).³⁹ The values of the CVs at the initial folded configuration are marked with black stars. We define the first-passage criterion as reaching a value $< 0.8\text{ nm}$ for the HLDA-based CV (dashed black line). This process has an estimated MFPT of $\sim 376\text{ ns}$ (see SI for details). We note, however, that the dynamics for reaching a stable unfolded state ($\text{HLDA} < 0.2\text{ nm}$) leads to a MFPT that is longer by an order of magnitude.²² However, since the underlying assumptions of iMetaD are valid for escaping a single energy well, we limit our discussion

to overcoming the first energy barrier along the HLDA-based CV. In addition, we note that the suboptimal CVs do not have a second minima in the FES for the stable unfolded state. Moreover, they do not fully distinguish between the unfolded and folded states. Therefore, even we biasing the suboptimal CVs, we use the value of the HLDA-based CV to determine the FPTs. The dotted lines in the middle and right panels of Figure 4(a), show the average values of those CVs when the first-passage criterion is fulfilled.

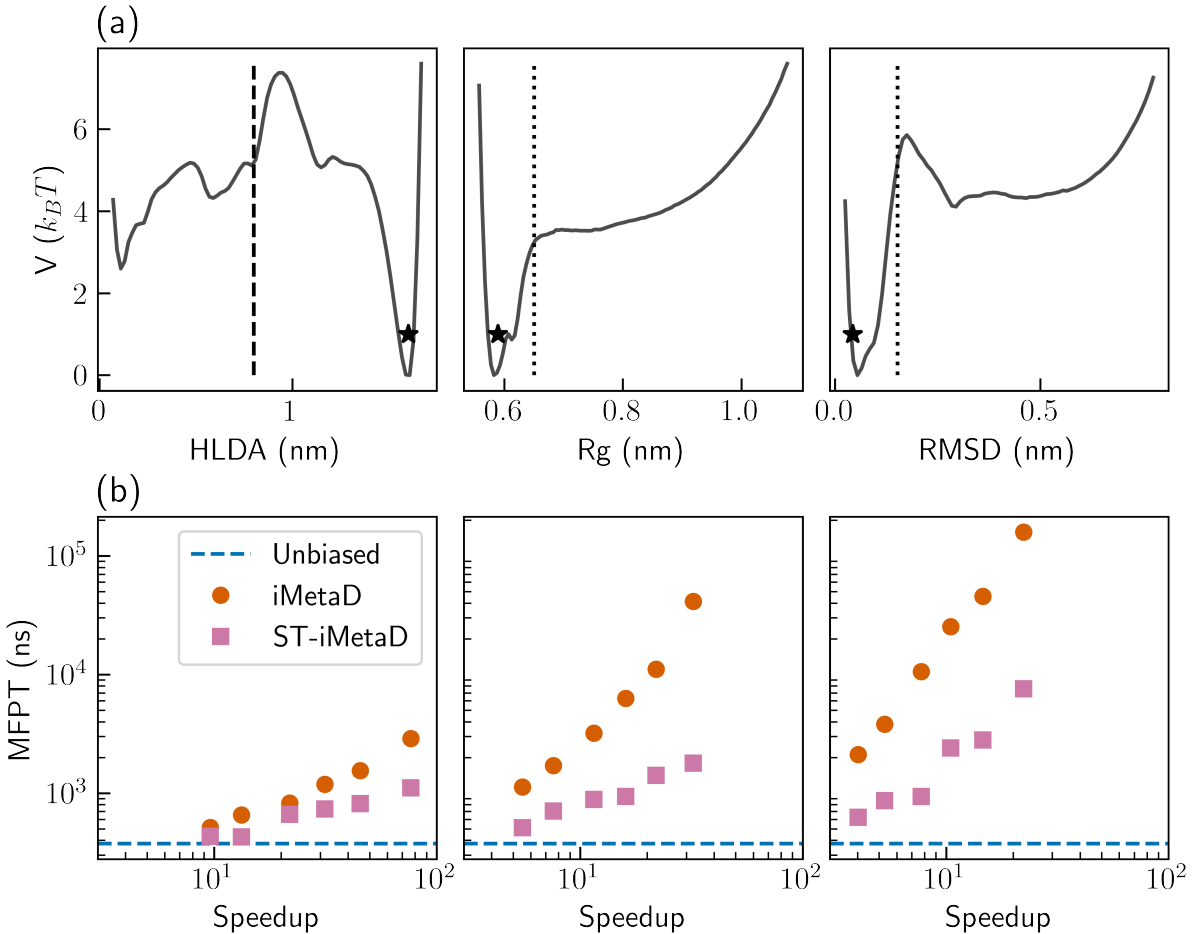


Figure 4: (a) Free-energy of solvated chignolin along the HLDA-based CV (left), the radius of gyration (middle) and the C-alpha RMSD (right). The vertical dashed line marks the first-passage criterion. The dotted vertical lines mark the average radius of gyration and C-alpha RMSD at first-passage events. (b) Estimated MFPTs obtained with standard iMetaD (orange circles) and ST-iMetaD (pink squares), using the HLDA-based CV (left), the radius of gyration (middle) and the C-alpha RMSD (right).

Figure 4(b) shows the estimated MFPT as a function of speedup, using the different CVs, with bias deposition rates in the range of 1 to 50 ns^{-1} . We observe similar trends as in the previous examples. In all cases, we find that ST-iMetaD leads to a better tradeoff between speedup and accuracy. Most notably, it is able to predict the MFPT rather successfully even for deposition rates where the standard approach leads to large errors.

To summarize, we present ST-iMetaD – an improved inference scheme for iMetaD simulations. We find that the rescaled FPT distribution provides the correct short-time statistics, even for high bias deposition rates and suboptimal CVs. By focusing on these timescales, the time-independent rate of Poisson processes can be estimated reliably, resulting in a better tradeoff between speedup and accuracy in predicting the unbiased MFPTs.

The benefits of ST-iMetaD are demonstrated for the Wolfe-Quapp potential and two molecular systems, an isolated alanine dipeptide molecule and chignolin in explicit water. It reduces the prediction errors by orders of magnitude, especially for simulations with frequent bias deposition or suboptimal CVs. As a result, our method significantly extends the range of applicability of iMetaD, though it will eventually also break for unrealistically high deposition rates or exceedingly bad CVs. The ST-iMetaD scheme can be applied in post-processing of existing iMetaD data, with no additional cost in comparison to the standard approach. Since it leads to either improved or comparable accuracy as iMetaD, by construction, we hope it would be widely adopted by the community. Furthermore, the inference scheme is not limited to iMetaD, and could be applied to any enhanced sampling approach based on the iMetaD rescaling scheme, such as OPES-flooding²² or Variational Flooding.^{40,41}

Data Availability

Example input files are available in the GitHub repository: <https://github.com/OfirBlumer/ST-iMetaD>.

Acknowledgement

Barak Hirshberg acknowledges support by the Israel Science Foundation (grants No. 1037/22 and 1312/22) and the Pazy Foundation of the IAEC-UPBC (grant No. 415-2023). Shlomi Reuveni acknowledges support from the Israel Science Foundation (grant No. 394/19). This project has received funding from the European Research Council (ERC) under the European Union’s Horizon 2020 research and innovation program (grant agreement No. 947731).

References

- (1) Tiwary, P.; Parrinello, M. From Metadynamics to Dynamics. *Phys. Rev. Lett.* **2013**, *111*, 230602.
- (2) Salvalaglio, M.; Tiwary, P.; Parrinello, M. Assessing the Reliability of the Dynamics Reconstructed from Metadynamics. *J. Chem. Theory. Comput.* **2014**, *10*, 1420–1425.
- (3) Valsson, O.; Tiwary, P.; Parrinello, M. Enhancing Important Fluctuations: Rare Events and Metadynamics from a Conceptual Viewpoint. *Annu. Rev. Phys. Chem.* **2016**, *67*, 159–184.
- (4) Palacio-Rodriguez, K.; Vroylandt, H.; Stelzl, L. S.; Pietrucci, F.; Hummer, G.; Cossio, P. Transition Rates and Efficiency of Collective Variables from Time-Dependent Biased Simulations. *J. Phys. Chem. Lett.* **2022**, *13*, 7490–7496.
- (5) Ray, D.; Parrinello, M. Kinetics from Metadynamics: Principles, Applications, and Outlook. *J. Chem. Theory. Comput.* **2023**, *acs.jctc.3c00660*.
- (6) Faradjian, A. K.; Elber, R. Computing Time Scales from Reaction Coordinates by Milestoning. *J. Chem. Phys.* **2004**, *120*, 10880–10889.
- (7) Elber, R. Milestoning: An Efficient Approach for Atomically Detailed Simulations of Kinetics in Biophysics. *Annu. Rev. Biophys.* **2020**, *49*, 69–85.

- (8) Bowman, G. R., Pande, V. S., Noé, F., Eds. *An Introduction to Markov State Models and Their Application to Long Timescale Molecular Simulation*; Advances in Experimental Medicine and Biology; Springer Netherlands: Dordrecht, 2014; Vol. 797.
- (9) Husic, B. E.; Pande, V. S. Markov State Models: From an Art to a Science. *J. Am. Chem. Soc.* **2018**, *140*, 2386–2396.
- (10) Blumer, O.; Reuveni, S.; Hirshberg, B. Stochastic Resetting for Enhanced Sampling. *J. Phys. Chem. Lett.* **2022**, *13*, 11230–11236.
- (11) Blumer, O.; Reuveni, S.; Hirshberg, B. Combining Stochastic Resetting with Metadynamics to Speed-up Molecular Dynamics Simulations. *Nat. Commun.* **2024**, *15*, 240.
- (12) Torrie, G.; Valleau, J. Nonphysical Sampling Distributions in Monte Carlo Free-Energy Estimation: Umbrella Sampling. *J. Comput. Phys.* **1977**, *23*, 187–199.
- (13) Kästner, J. Umbrella sampling: Umbrella sampling. *Wiley Interdiscip. Rev.: Comput. Mol. Sci.* **2011**, *1*, 932–942.
- (14) Grubmüller, H. Predicting Slow Structural Transitions in Macromolecular Systems: Conformational Flooding. *Phys. Rev. E* **1995**, *52*, 2893–2906.
- (15) Rosso, L.; Tuckerman, M. E. An Adiabatic Molecular Dynamics Method for the Calculation of Free Energy Profiles. *Mol. Simul.* **2002**, *28*, 91–112.
- (16) Rosso, L.; Mináry, P.; Zhu, Z.; Tuckerman, M. E. On the Use of the Adiabatic Molecular Dynamics Technique in the Calculation of Free Energy Profiles. *J. Chem. Phys.* **2002**, *116*, 4389–4402.
- (17) Abrams, J. B.; Tuckerman, M. E. Efficient and Direct Generation of Multidimensional Free Energy Surfaces via Adiabatic Dynamics without Coordinate Transformations. *J. Phys. Chem. B* **2008**, *112*, 15742–15757.

- (18) Invernizzi, M.; Parrinello, M. Rethinking Metadynamics: From Bias Potentials to Probability Distributions. *J. Phys. Chem. Lett.* **2020**, *11*, 2731–2736.
- (19) Invernizzi, M.; Parrinello, M. Exploration vs Convergence Speed in Adaptive-Bias Enhanced Sampling. *J. Chem. Theory. Comput.* **2022**, *18*, 3988–3996.
- (20) Barducci, A.; Bonomi, M.; Parrinello, M. Metadynamics. *Wiley Interdiscip. Rev.: Comput. Mol. Sci.* **2011**, *1*, 826–843.
- (21) Sutto, L.; Marsili, S.; Gervasio, F. L. New Advances in Metadynamics. *Wiley Interdiscip. Rev.: Comput. Mol. Sci.* **2012**, *2*, 771–779.
- (22) Ray, D.; Ansari, N.; Rizzi, V.; Invernizzi, M.; Parrinello, M. Rare Event Kinetics from Adaptive Bias Enhanced Sampling. *J. Chem. Theory. Comput.* **2022**, *18*, 6500–6509.
- (23) Invernizzi, M.; Parrinello, M. Making the Best of a Bad Situation: A Multiscale Approach to Free Energy Calculation. *J. Chem. Theory. Comput.* **2019**, *15*, 2187–2194.
- (24) Dietschreit, J. C. B.; Diestler, D. J.; Gómez-Bombarelli, R. Entropy and Energy Profiles of Chemical Reactions. *J. Chem. Theory. Comput.* **2023**, *19*, 5369–5379, PMID: 37535443.
- (25) Mendels, D.; Piccini, G.; Brotzakis, Z. F.; Yang, Y. I.; Parrinello, M. Folding a Small Protein Using Harmonic Linear Discriminant Analysis. *J. Chem. Phys.* **2018**, *149*, 194113.
- (26) Mendels, D.; Piccini, G.; Parrinello, M. Collective Variables from Local Fluctuations. *J. Phys. Chem. Lett.* **2018**, *9*, 2776–2781.
- (27) Bonati, L.; Piccini, G.; Parrinello, M. Deep Learning the Slow Modes for Rare Events Sampling. *Proc. Natl. Acad. Sci. U. S. A.* **2021**, *118*, e2113533118.

- (28) Sidky, H.; Chen, W.; Ferguson, A. L. Machine Learning for Collective Variable Discovery and Enhanced Sampling in Biomolecular Simulation. *Mol. Phys.* **2020**, *118*, e1737742.
- (29) Chen, M. Collective Variable-Based Enhanced Sampling and Machine Learning. *Eur. Phys. J. B* **2021**, *94*, 211.
- (30) Liu, B.; Xue, M.; Qiu, Y.; Konovalov, K. A.; O'Connor, M. S.; Huang, X. Graph-VAMPnets for Uncovering Slow Collective Variables of Self-Assembly Dynamics. *J. Chem. Phys.* **2023**, *159*, 094901.
- (31) Sasmal, S.; McCullagh, M.; Hocky, G. M. Reaction Coordinates for Conformational Transitions Using Linear Discriminant Analysis on Positions. *J. Chem. Theory. Comput.* **2023**, *19*, 4427–4435, PMID: 37130367.
- (32) Massey, F. J. The Kolmogorov-Smirnov Test for Goodness of Fit. *J. Am. Stat. Assoc.* **1951**, *46*, 68–78.
- (33) Bolhuis, P. G.; Chandler, D.; Dellago, C.; Geissler, P. L. Transition Path Sampling: Throwing Ropes Over Rough Mountain Passes, in the Dark. *Annu. Rev. Phys. Chem.* **2002**, *53*, 291–318.
- (34) Peters, B. In *Reaction Rate Theory and Rare Events Simulations*; Peters, B., Ed.; Elsevier: Amsterdam, 2017; pp 539–571.
- (35) Lindorff-Larsen, K.; Piana, S.; Dror, R. O.; Shaw, D. E. How Fast-Folding Proteins Fold. *Science* **2011**, *334*, 517–520.
- (36) Miao, Y.; Feher, V. A.; McCammon, J. A. Gaussian Accelerated Molecular Dynamics: Unconstrained Enhanced Sampling and Free Energy Calculation. *J. Chem. Theory. Comput.* **2015**, *11*, 3584–3595.

- (37) Shaffer, P.; Valsson, O.; Parrinello, M. Enhanced, Targeted Sampling of High-Dimensional Free-Energy Landscapes Using Variationally Enhanced Sampling, with an Application to Chignolin. *Proc. Natl. Acad. Sci. U. S. A.* **2016**, *113*, 1150–1155.
- (38) Wang, D.; Wang, Y.; Chang, J.; Zhang, L.; Wang, H.; E., W. Efficient Sampling of High-Dimensional Free Energy Landscapes Using Adaptive Reinforced Dynamics. *Nat. Comput. Sci.* **2022**, *2*, 20–29.
- (39) Grossfield, A. WHAM: The Weighted Histogram Analysis Method, Version 2.0.11. http://membrane.urmc.rochester.edu/wordpress/?page_id=126, Accessed: October 17, 2023.
- (40) McCarty, J.; Valsson, O.; Tiwary, P.; Parrinello, M. Variationally Optimized Free-Energy Flooding for Rate Calculation. *Phys. Rev. Lett.* **2015**, *115*, 070601.
- (41) Piccini, G.; McCarty, J. J.; Valsson, O.; Parrinello, M. Variational Flooding Study of a SN2 Reaction. *J. Phys. Chem. Lett.* **2017**, *8*, 580–583, PMID: 28071915.

Supporting Information:

Short-Time Infrequent Metadynamics for Improved Kinetics Inference

Ofir Blumer,[†] Shlomi Reuveni,^{†,‡,¶} and Barak Hirshberg^{*,†,‡}

[†]*School of Chemistry, Tel Aviv University, Tel Aviv 6997801, Israel.*

[‡]*The Center for Computational Molecular and Materials Science, Tel Aviv University, Tel Aviv 6997801, Israel.*

[¶]*The Center for Physics and Chemistry of Living Systems, Tel Aviv University, Tel Aviv 6997801, Israel.*

E-mail: hirshb@tauex.tau.ac.il

Simulation details

Here we give the setup for all molecular dynamics (MD) and Metadynamics (MetaD) simulations presented in the main text. In all cases, we report averages over 1000 independent trajectories, except for unbiased MD simulations of chignolin, where only 200 trajectories were sampled.

The Wolfe-Quapp potential

Simulations of the Wolfe-Quapp potential were performed in the Large-scale Atomic/Molecular Massively Parallel Simulator (LAMMPS).^{S1} We followed the motion of a single particle with mass $m = 40 \text{ a.u.}$ The simulations were carried out in the canonical (NVT) ensemble at a

temperature of 300 K , using a Langevin thermostat.^{S2} The integration timestep was 1 fs and the friction coefficient was 0.01 fs^{-1} . Infrequent MetaD (iMetaD) was implemented using PLUMED 2.7.1.^{S3–S5} We used a bias height of $0.5\text{ }k_B T$, bias factor of 5, bias width of $\sigma = 0.1\text{ nm}$ and grid spacing of 0.01 nm .

The external potential was implemented in the LAMMPS input files. Its structure is as described in previous publications,^{S6,S7} and is shown in Figure S1. The exact form used is given in Eq. 1, with the distance given in units of nm and the energy in units of $1\text{ }k_B T$:

$$V(x, y) = x^4 + y^4 - 4x^2 - 2y^2 + 2xy + 0.1x + 0.8y \quad (1)$$

Simulations were initiated from the global minimum ($x = 1.564, y = -1.334\text{ nm}$, marked with a star in Figure S1, with velocities sampled from the Maxwell Boltzmann distribution. All trajectories were stopped using the COMMITTOR command in PLUMED when reaching the second local minima, defined as $x < -1.4\text{ nm} \wedge y > 1.0\text{ nm}$, denoted by dashed lines in Figure S1.

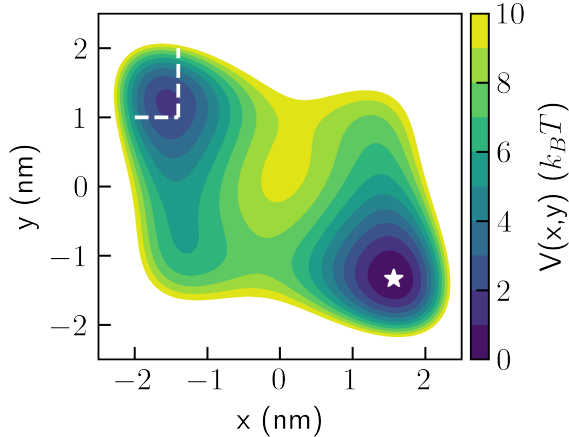


Figure S1: The Wolfe-Quapp potential. The starting position is marked with a star, and the target basin is marked with dashed lines.

Alanine dipeptide

Simulations of alanine dipeptide in vacuum were performed in GROMACS 2019.6.^{S8} We used input files by Bonomi and Bussi,^{S9} implementing the AMBER99SB force field (FF). Simulations were performed in the NVT ensemble at a temperature of 300 K , using a stochastic velocity rescaling thermostat.^{S10} The integration time step was 2 fs . Infrequent Meta-dynamics (iMetaD) was implemented once more using PLUMED. We used a bias height of $0.5\text{ }k_BT$, bias factor of 5, bias width of $\sigma = 0.25\text{ rad}$ and grid spacing of 0.01 rad . All trajectories were initiated in a fixed position at the C_{7eq} conformer and stopped using PLUMED when reaching $0.5 < \phi < 1.5\text{ rad}$. The stopping criterion was checked every 1 ps .

Chignolin

Simulations of chignolin in water were performed using the same software as those of alanine dipeptide. We used input files by Ray et. al.,^{S7} available at PLUMED-NEST, the public repository of the PLUMED consortium,^{S5} as plumID:22.031. We used the CHARMM22* FF^{S11} for the protein and the CHARMM TIP3P FF^{S12} for water. The thermodynamic ensemble, thermostat and integration timestep were the same as employed for alanine dipeptide, but the temperature was higher, 340 K .

We used three collective variables (CVs) for the iMetaD simulations: the radius of gyration (Rg), the C-alpha root-mean-squared deviation from the folded state (RMSD), and a CV based on harmonic linear discriminant analysis (HLDA).^{S13} We used a bias height of $0.5\text{ }k_BT$, bias factor of 5 and grid spacing of 0.001 nm for all CVs. The bias width was 0.022 , 0.005 and 0.006 nm for the HLDA, Rg and RMSD-based CVs, respectively. All trajectories were initiated from a fixed position and stopped using PLUMED when reaching $s < 0.8\text{ nm}$, with s being the HLDA-based CV. This stopping criterion was checked every 1 ps .

Committer analysis

Here we report the details of the committer analysis performed to estimate the quality of different CVs for the Wolfe-Quapp potential. Our procedure is based on that described by Peters.^{S14} We defined two states, A at $x > 1.4 \text{ nm}$, $y < -1.0 \text{ nm}$ and B at $x < -1.4 \text{ nm}$ and $y > 1.0 \text{ nm}$. For each examined CV $s(x, y)$, we first performed a 10 ns long simulation initiated at $(x = 0, y = 0) \text{ nm}$, restricted to $s \approx 0 \text{ nm}$ by a bias potential $V(s) = 80s^2$, with $V(s)$ in units of $1 k_B T$ and s in nm . A thousand uncorrelated configurations were randomly sampled from the restricted trajectory, to serve as new initial configurations. Next, for each initial configuration, we sampled 100 trajectories and obtained the fraction of trajectories that reached the target state B before state A , p_B .

Finally, we examined the histogram of p_B for all tested CVs. The CV showing the narrowest distribution around $p_B = 0.5$ best approximates the true committer, and is regarded in the main text as the good CV. It is given by $s(x, y) = \cos\left(\frac{\pi}{9}\right)x + \sin\left(\frac{\pi}{9}\right)y$. Figure S2 shows the histograms of p_B for this CV and for $s(x, y) = x$, which is a poor CV, for comparison.

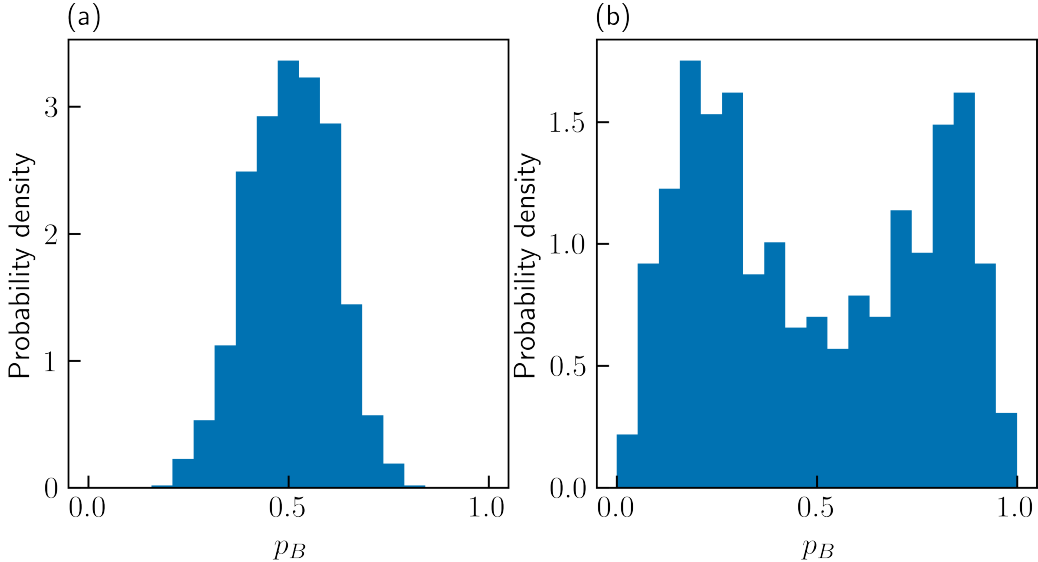


Figure S2: Histograms of p_B for (a) the good CV and (b) a poor CV.

Mean first-passage time estimation

Here we explain how the unbiased mean first-passage time (MFPT) values of the different processes were evaluated. For all systems, we first performed standard MD simulations, that were stopped when the first-passage criterion was fulfilled. For the Wolfe-Quapp potential, all trajectories exhibited a first-passage. The MFPT was simply taken as the average first-passage time (FPT) of all trajectories. However, for both molecular systems, $\sim 7\%$ of the simulations did not show a first-passage event. Therefore, taking the MFPT of all trajectories would underestimate the true value.

Instead, we used the assumption that the FPT distribution is exponential. We made a linear fit to the logarithm of the survival function, and evaluated the true MFPT as $-k^{-1}$, with k being the slope of the fit. For both systems, we obtained high coefficient of determination values, $R^2 > 0.995$, confirming that the underlying distributions are exponential.

Free-energy inference

Here we report the details of how we obtained the free-energy surfaces (FES) featured in Figure 4(a) of the main text. For each CV, we performed 32, 100 ns long umbrella sampling simulations,^{S15,S16} with harmonic constraints centered at $s_{min} + i\Delta_s$, with i going from 0 to 31. We used $s_{min} = 0.5, 6, 0.25 \text{ \AA}$ and $\Delta_s = 0.5, 0.167, 0.25 \text{ \AA}$ for the HLDA, Rg and RMSD based CVs, respectively. The harmonic constant was $k = 3 k_B T \text{ \AA}^{-2}$ for all CVs. We value of the CV was saved every 1 ps , and the FES was constructed through the Weighted Histogram Analysis Method (WHAM), using the implementation of Grossfield.^{S17}

References

- (S1) Thompson, A. P.; Aktulga, H. M.; Berger, R.; Bolintineanu, D. S.; Brown, W. M.; Crozier, P. S.; in 't Veld, P. J.; Kohlmeyer, A.; Moore, S. G.; Nguyen, T. D.; Shan, R.;

- Stevens, M. J.; Tranchida, J.; Trott, C.; Plimpton, S. J. LAMMPS - A Flexible Simulation Tool for Particle-Based Materials Modeling at the Atomic, Meso, and Continuum Scales. *Comp. Phys. Comm.* **2022**, *271*, 108171.
- (S2) Schneider, T.; Stoll, E. Molecular-Dynamics Study of a Three-Dimensional One-Component Model for Distortive Phase Transitions. *Phys. Rev. B* **1978**, *17*, 1302–1322.
- (S3) Bonomi, M.; Branduardi, D.; Bussi, G.; Camilloni, C.; Provati, D.; Raiteri, P.; Donadio, D.; Marinelli, F.; Pietrucci, F.; Broglia, R. A.; Parrinello, M. PLUMED: A Portable Plugin for Free-Energy Calculations with Molecular Dynamics. *Comp. Phys. Comm.* **2009**, *180*, 1961–1972.
- (S4) Tribello, G. A.; Bonomi, M.; Branduardi, D.; Camilloni, C.; Bussi, G. PLUMED 2: New Feathers for an Old Bird. *Comp. Phys. Comm.* **2014**, *185*, 604–613.
- (S5) The PLUMED Consortium, Promoting Transparency and Reproducibility in Enhanced Molecular Simulations. *Nat. Methods* **2019**, *16*, 670–673.
- (S6) Invernizzi, M.; Parrinello, M. Making the Best of a Bad Situation: A Multiscale Approach to Free Energy Calculation. *J. Chem. Theory. Comput.* **2019**, *15*, 2187–2194.
- (S7) Ray, D.; Ansari, N.; Rizzi, V.; Invernizzi, M.; Parrinello, M. Rare Event Kinetics from Adaptive Bias Enhanced Sampling. *J. Chem. Theory. Comput.* **2022**, *18*, 6500–6509.
- (S8) Abraham, M. J.; Murtola, T.; Schulz, R.; Páll, S.; Smith, J. C.; Hess, B.; Lindahl, E. GROMACS: High Performance Molecular Simulations Through Multi-Level Parallelism from Laptops to Supercomputers. *SoftwareX* **2015**, *1-2*, 19–25.
- (S9) Bonomi, M.; Bussi, G. PLUMED: Munster Tutorial. 2015; <https://www.plumed.org/doc-v2.7/user-doc/html/munster.html>, Accessed:.

- (S10) Bussi, G.; Donadio, D.; Parrinello, M. Canonical Sampling Through Velocity Rescaling. *J. Chem. Phys.* **2007**, *126*, 014101.
- (S11) Piana, S.; Lindorff-Larsen, K.; Shaw, D. How Robust Are Protein Folding Simulations with Respect to Force Field Parameterization? *Biophys. J.* **2011**, *100*, L47–L49.
- (S12) MacKerell, A. D.; Bashford, D.; Bellott, M.; Dunbrack, R. L.; Evanseck, J. D.; Field, M. J.; Fischer, S.; Gao, J.; Guo, H.; Ha, S.; Joseph-McCarthy, D.; Kuchnir, L.; Kuczera, K.; Lau, F. T. K.; Mattos, C.; Michnick, S.; Ngo, T.; Nguyen, D. T.; Prodhom, B.; Reiher, W. E.; Roux, B.; Schlenkrich, M.; Smith, J. C.; Stote, R.; Straub, J.; Watanabe, M.; Wiórkiewicz-Kuczera, J.; Yin, D.; Karplus, M. All-Atom Empirical Potential for Molecular Modeling and Dynamics Studies of Proteins. *J. Phys. Chem. B* **1998**, *102*, 3586–3616.
- (S13) Mendels, D.; Piccini, G.; Brotzakis, Z. F.; Yang, Y. I.; Parrinello, M. Folding a Small Protein Using Harmonic Linear Discriminant Analysis. *J. Chem. Phys.* **2018**, *149*, 194113.
- (S14) Peters, B. In *Reaction Rate Theory and Rare Events Simulations*; Peters, B., Ed.; Elsevier: Amsterdam, 2017; pp 539–571.
- (S15) Torrie, G.; Valleau, J. Nonphysical Sampling Distributions in Monte Carlo Free-Energy Estimation: Umbrella Sampling. *J. Comput. Phys.* **1977**, *23*, 187–199.
- (S16) Kästner, J. Umbrella sampling: Umbrella sampling. *Wiley Interdiscip. Rev.: Comput. Mol. Sci.* **2011**, *1*, 932–942.
- (S17) Grossfield, A. WHAM: The Weighted Histogram Analysis Method, Version 2.0.11. http://membrane.urmc.rochester.edu/wordpress/?page_id=126, Accessed: October 17, 2023.